

Line-Defect Patterns of Unstable Spiral Waves in Cardiac Tissue

Juan G. Restrepo¹ and Alain Karma¹

¹Department of Physics and Center for Interdisciplinary Research on Complex Systems, Northeastern University, Boston, MA, 02115 USA

(Dated: November 13, 2018)

Spiral wave propagation in period-2 excitable media is often accompanied by line-defects, the locus of points with period-1 oscillations. Here we investigate spiral line-defects in cardiac tissue where period-2 behavior has a known arrhythmogenic role. We find that the number of line defects, which is constrained to be an odd integer, is three for a freely rotating spiral, with and without meander, but one for a spiral anchored around a fixed heterogeneity. We interpret analytically this finding using a simple theory where spiral wave unstable modes with different numbers of line-defects correspond to quantized solutions of a Helmholtz equation. Furthermore, the slow inward rotation of spiral line-defects is described in different regimes.

Spiral waves are observed in extremely diverse physical and biological excitable media and are known to play a key role in the genesis of abnormally rapid life-threatening heart rhythm disorders [1]. Despite considerable progress to date, complex spatiotemporal behaviors resulting from unstable spiral wave propagation remain poorly understood theoretically with the exception of meander [2, 3], a classic spiral core instability with flower-like tip trajectories. A particularly rich dynamics results from instabilities in period-2 media where the local dynamics of the medium, i.e. the dynamics of uncoupled excitable elements, exhibits a period-doubling bifurcation as a function of parameters of the medium or the external stimulation frequency. Although period-2 behavior has been seen in different excitable and oscillatory media, it has received particular attention in a cardiac context. The hallmark of period-2 behavior in this context is alternans, a beat-to-beat alternation in the duration of cardiac excitation, which has been linked to the onset of lethal heart rhythm disorders [4].

Unstable spiral wave propagation in period-2 media is invariably accompanied by “line-defects”, which are the locus of points where the dynamics is locally period-1. Line-defects are generally present in these media when plane waves radiating out of the core region are unstable at the spiral rotation period, independently of whether meander is present or not. Studies in *in vitro* cardiac cell tissue cultures [5, 6], chemical reactions [7, 8, 9], and coupled oscillators [10, 11] have revealed the existence of a rich variety of patterns ranging from one and three line-defect structures [8], to phase bubbles [12], to line-defect turbulence [13]. Spiral wave breakup in models of cardiac excitation has also been found in parameter regimes of local period-2 dynamics, and hypothesized in this context as a potential mechanism for heart fibrillation [1, 14, 15, 16]. Spiral line-defect patterns, however, have not been systematically investigated in cardiac tissue.

In this Letter, we investigate the selection and dynamics of line-defect patterns resulting from unstable spiral wave propagation in cardiac tissue. Moreover, we interpret our findings using an amplitude equation framework recently used to study the evolution of line-defects during periodic stimulation from a single site [17]. In this framework, the spatiotemporal modulation of the phase and amplitude of period-2 oscillations is described by a simple partial differential equation that can be

readily analyzed. Our study is based on the standard wave equation for cardiac tissue

$$\partial_t V = \gamma \nabla^2 V - I_m(V, \vec{y})/C_m, \quad (1)$$

where V is the transmembrane voltage, γ is the voltage diffusion coefficient, C_m is the membrane capacitance, and \vec{y} is a vector of gate variables that controls the flow of ions through the membrane, and hence the total membrane ionic current I_m . We studied different models of $I_m(V, \vec{y})$ and gating kinetics to explore universal features of line-defect patterns that depend on qualitative properties of core and plane wave instabilities. The latter are manifested either as *stationary* [17, 18] or *traveling* [17] spatial modulations of period-2 oscillation amplitude with an intrinsic spatial scale determined by parameters of the excitable medium [17]. These spatial modulations have nodes with period-1 dynamics in one dimension, or nodal lines in two, which correspond here to line-defects in the spiral far-field. We therefore chose models to explore line-defect patterns for stationary and traveling nodes with and without meander. The model of Ref. [15] has pinwheel spirals (no meander) and stationary nodes under periodic pacing. The other two models of Ref. [19] and Ref. [17] both exhibit meander and have fixed and traveling nodes, respectively.

Freely propagating spiral waves in all three models were studied by numerically solving Eq. (1) in a circular domain of radius $r_e = 3$ cm with no-flux boundary condition, $\partial_r V|_{r=r_e} = 0$. Anchored spirals were studied by introducing an inexcitable disk of radius r_i and imposing no-flux conditions on both the inner and outer radii, $\partial_r V|_{r=r_i} = \partial_r V|_{r=r_e} = 0$. We implemented the phase-field method of Ref. [20] that automatically handles no-flux boundary conditions in an arbitrary geometry using a finite-difference representation of the Laplacian on a square grid, and iterated Eq. (1) using a simple explicit Euler scheme. Model parameters are identical to the published ones except those listed in Fig. 1. The latter were chosen for intermediate action potential duration restitution slopes, which suffice to produce unstable spiral waves with line-defects in each geometry, but are not steep enough to cause wave breakup in this domain size.

We used a half plane wave as initial condition to initiate a spiral wave (obtained by first triggering a full plane wave and resetting part of the circular domain to the resting state). To

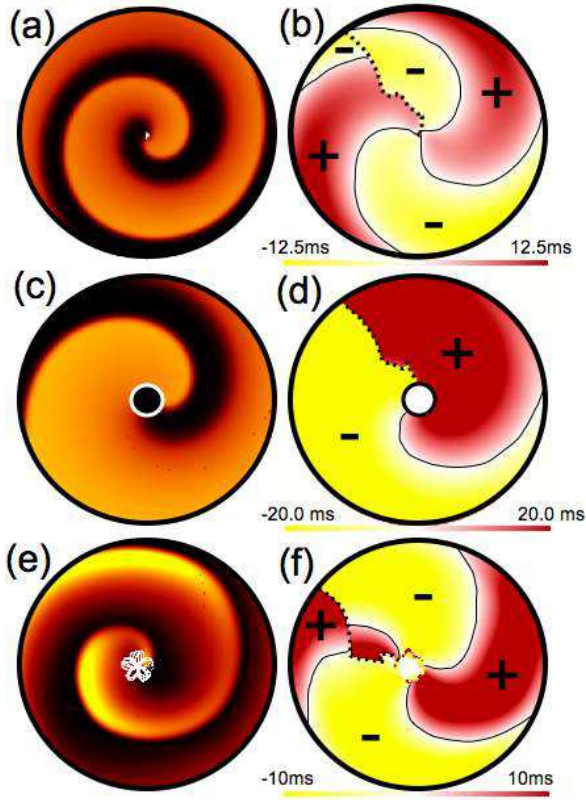


FIG. 1: Membrane voltage (left) and corresponding alternans amplitude a (right) for different ionic models and geometries: model of Ref. [15] without (a and b; $Re = 1.15$) and with a circular inexcitable disk of radius $r_i = 0.5$ cm (c and d; $Re = 1.25$), and model of Ref. [19] without disk (e and f; $t_{f2} = 30$ ms, $t_{si} = 10$ ms, $t_{h2} = 2.0$ ms). In panels (a), (c), and (e), grey (orange online) indicates depolarization, and white indicates the trajectory of the spiral tip. In panels (b), (d), and (f), dark grey (red online) and light grey (yellow online) correspond to $a > 0$ and $a < 0$ regions, separated by line-defects (solid lines); the grey (color online) scale does not vary outside the indicated range of a . Line-defects in (b), (d), and (f), rotate counterclockwise with a period that is approximately 17, 8, and 9 times the clockwise spiral rotation period in (a), (c), and (e), respectively. The discontinuity of a across the dashed line is a consequence of the definition of the common beat number (see text).

track line defects, we define at each point \mathbf{x} and time t a local beat number $n(\mathbf{x}, t)$, set everywhere initially to zero after the half plane wave is created, and increased by one at the end of each action potential, i.e. every time that the voltage $V(\mathbf{x}, t)$ crosses a fixed threshold V_c with $dV/dt < 0$. We then define the period-2 alternans amplitude as

$$a(\mathbf{x}, t) = (-1)^{n_c(t)} [D(\mathbf{x}, n_c(t)) - D(\mathbf{x}, n_c(t) - 1)] / 2 \quad (2)$$

where $D(\mathbf{x}, n) = \int_{V(\mathbf{x}, t) > V_c, n(\mathbf{x}, t) = n-1} dt'$ is the local action potential duration (APD) and $n_c(t) \equiv \min_{\mathbf{x}} n(\mathbf{x}, t)$ is the common beat, i.e. the largest beat number that has been registered at all points at time t . The line-defects are then the locus of points where $a(\mathbf{x}, t) = 0$ at any instant of time. The use of a common beat number introduces here a discontinuity in a (indicated by dashed lines in Fig. 1) since the APD of a given beat might change as the wave front rotates around the spiral

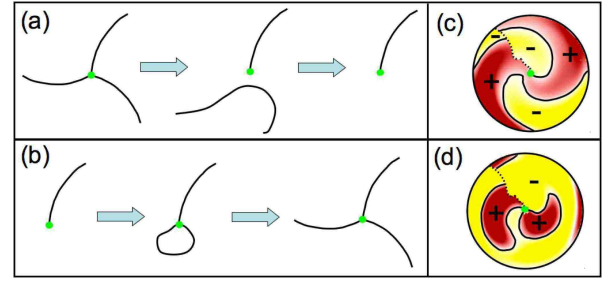


FIG. 2: Schematic illustration of transitions from (a) three to one and (b) one to three line-defects and corresponding examples from simulations of the model of Ref. [15] with the same conventions and parameters as in Fig. 1 (b). The small circle (green online) in (a) and (b) represents the spiral core region or a small anchoring obstacle.

tip. This discontinuity, however, does not affect the dynamics. Other methods to track line defects [7, 21] yield similar results except for unessential imaging differences.

Results of simulations that pertain to the selection of the number of line-defects are shown in Fig. 1. The top four panels reveal that the pinwheel spirals simulated with the two-variable model of Ref. [15] exhibit three line-defects when propagating freely in spatially homogeneous tissue, but only one line-defect when anchored around an inexcitable disk of 0.5 cm radius. Furthermore, the bottom two panels show that for the more physiologically realistic three-variable model of Ref. [19], freely propagating spirals still exhibit three-line defects even though the spiral tip meanders.

Since anchored spirals become free in the limit of vanishing obstacle size, one would expect transitions from one to three (three to one) line-defects to occur with decreasing (increasing) obstacle size. Indeed, for the model of Ref. [15], we found three line defects for obstacles with diameter smaller than ~ 0.1 cm, including the freely propagating pinwheel spiral ($r_i = 0$) in Fig. 1 (b), and one line defect for diameters larger than ~ 0.3 cm as in the example of Fig. 1 (d). For intermediate diameters, we found complex behaviors marked by transitions from three to one or one to three line-defects. The former occur when two line defects merge into one line defect that moves away from the core, and the latter when a phase bubble enclosed by a line-defect loop nucleates in, and expands from, the core, as illustrated in Fig. 2. We find the same qualitative behavior in the model of Ref. [19] except that meander makes the transitions between patterns with different numbers of line-defects more complex.

Let us now turn to interpret our results in the amplitude equation framework [17]. For simplicity, we restrict our analysis to non-meandering spiral waves. Furthermore, to keep the analysis tractable, we first assume that the propagation wave speed is constant and relax this assumption subsequently when examining the motion of line defects. With this assumption, linear perturbations of a steady-state rigidly rotating spiral wave with period T obey the equation

$$T \partial_t a = \sigma a + \xi^2 \nabla^2 a, \quad (3)$$

where a is the alternans amplitude subject to the radial

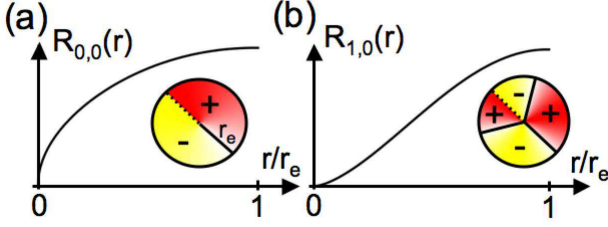


FIG. 3: Theoretical radial and angular (insets) dependence of the alternans amplitude for (a) 1 and (b) 3 line defect modes.

$\partial_r a|_{r_i} = \partial a|_{r_e} = 0$ and angular $a(\theta + 2\pi, t) = -a(\theta, t)$ boundary conditions. The latter constrains the number of line defects to be an odd integer and results from the change in beat number across any closed circuit enclosing the spiral tip for steady-state alternans. It follows directly from the definition of a [Eq. (2)] and the requirement that the voltage be continuous everywhere in space. In addition, $\sigma = \ln f'$, where f' , the slope of the action potential duration restitution curve defined by $D^{n+1} = f(T - D^n)$, controls the onset of alternans and $\xi \sim (\gamma D)^{1/2}$, where D is the value of the action potential duration at the period-doubling bifurcation ($\sigma = 0$), measures the scale over which the voltage dynamics is diffusively coupled on the time scale of one beat.

This linear stability problem is easily solved by the substitution $a(\mathbf{r}, t) \sim e^{\Omega t} \Psi(r, \theta)$ that transforms Eq. (3) into a Helmholtz equation for $\Psi(r, \theta)$. The latter can then be solved by separation of variables with the substitution $\Psi(r, \theta) \sim R(r)\Theta(\theta)$. The angular part is found to be $\Theta_n(\theta) = \sin((n + 1/2)\theta)$, where mode n corresponds to $2n + 1$ line-defects. The radial part obeys a Bessel equation. For $r_i > 0$, it has solutions $R_{n,m}(r) \propto J'_{-n-1/2}(k_{n,m}r_e)J_{n+1/2}(k_{n,m}r) - J'_{n+1/2}(k_{n,m}r_e)J_{-n-1/2}(k_{n,m}r)$ that satisfy the outer radial boundary condition $\partial_r a|_{r_e} = 0$, where $n, m = 0, 1, \dots$, and the inner condition $\partial_r a|_{r_i} = 0$ determines $k_{n,m}$, and hence the growth rate $\Omega_{n,m}T = \sigma - \xi r_e^{-2} k_{n,m}^2$. We find that the smallest $k_{n,m}$ occurs for $n = 0$ independently of the ratio r_e/r_i . Therefore, the mode corresponding to a single line defect is the most unstable when the spiral is anchored. This agrees with our numerical observations in Fig. 1 (d). For freely rotating spirals, $r_i = 0$, $J_{-n-1/2}(r)$ diverges at the origin, so the solutions are $R_{n,m}(r) \propto J_{n+1/2}(k_{n,m}r)$, where $k_{nm}r_e$ is the m^{th} zero of $J'_n(r)$. The most unstable modes are $n = 0$ and $n = 1$ corresponding to 1 and 3 line defects, respectively (see Fig. 3). However, $J_{1/2}(k_{0,0}r)$ has a divergent derivative that is incompatible with the physical requirement that the voltage, and hence the APD, must vary smoothly on a scale ξ . On the other hand, $J_{3/2}(k_{1,0}r)$ smoothly vanishes at the origin. Therefore, in this case, the boundary condition at the origin selects a 3-line-defect pattern as observed in Fig. 1 (b). Interestingly, a 3-line-defect pattern is also selected with meander present [Fig. 1 (f)], thereby suggesting that the boundary condition on a on the outer scale of the line-defect pattern is not strongly affected by meander.

The analysis also predicts qualitative features of the radial distribution of alternans amplitude for three- and one-line-defect patterns of Figs. 1(b) and 1(d), respectively. Fig. 4

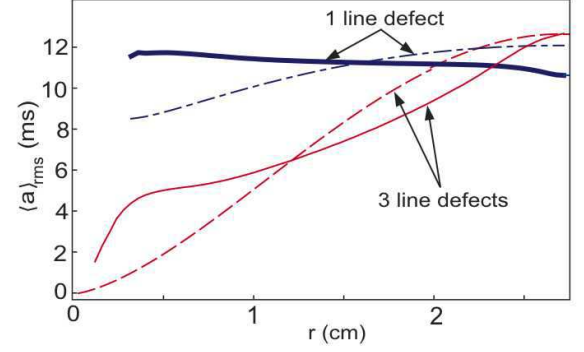


FIG. 4: $\langle a \rangle_{rms}$ versus radial distance r for the pinwheel spiral (thin solid line, red online) and anchored spiral (thick solid line, blue online), and respective theoretical radial modes $R_{1,0}(r)$ (thin dashed, red online), and $R_{0,0}(r)$ (dotted-dashed line, blue online). compares the numerical radial distributions of root-mean-square amplitude $\langle a \rangle_{rms}$ averaged over a full line-defect rotation period for three line-defects (thin solid line) and one line-defect (thick line), with the corresponding radial modes from the theoretical analysis (dashed lines) scaled to have the same radial average as the observed curves. The theory predicts well that the alternans amplitude is more strongly suppressed near the core for the larger number of line defects.

So far our analysis has assumed that the wave speed is constant, which predicts that line-defects extend straight out of the core and are stationary, as implied by the angular distribution $\sin((n + 1/2)\theta)$ of linearly unstable modes (see Fig. 3). In contrast, simulations in Fig. 1 show that line-defects have a spiral shape and slowly rotate inward in the opposite direction of the spiral wavefront. Line-defect motion can generally be induced both by line-defect curvature and the dependence of the wave speed c on the interval I between two waves, known as the conduction velocity (CV) restitution curve in the cardiac literature. While a full stability analysis that includes these effects would be required to treat line-defect motion in general, two important limiting cases can be readily analyzed.

The first pertains to anchored spiral waves for medium parameters where plane waves paced at the spiral rotation period exhibits stationary line-defects, as for the model of Ref. [15] studied here. In this case, we expect line-defect motion to be generated predominantly by the spiral wavefront dynamics around the anchoring obstacle. Neglecting wavefront curvature effects, this dynamics should be approximately described by that of a propagating pulse in a one-dimensional ring of perimeter $L = 2\pi r_i$ [17, 22]. To test this hypothesis, we computed the quasiperiodic frequency Ω of the local medium dynamics induced by line-defect rotation for anchored spirals for the model of Ref. [15]. The frequency was obtained by fitting the time series $a(\mathbf{r}, jT)/a(\mathbf{r}, 0)$ at a single point \mathbf{r} to $\eta^j \cos(\Omega T j + \delta)$, with η , Ω , and δ the fitting parameters. For the theory, we used the dispersion relation giving the quasiperiodic frequency Ω modulating alternans, $a \propto e^{i\Omega j T}$, in a one dimensional ring derived in Ref. [17]

$$e^{i\Omega T} \left(1 - \frac{i}{2\Lambda k} \right) = (1 - iwk - \xi^2 k^2) f'(I) + \frac{i}{2\Lambda k}, \quad (4)$$

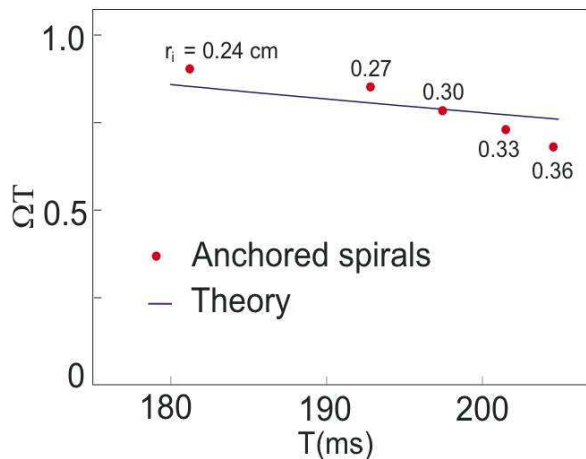


FIG. 5: Comparison of numerical (circles, red online) and theoretical (solid line) line-defect rotation frequencies for spiral waves anchored to disks of varying radii for the model of Ref. [15].

where $k = \pi/L + \Omega T/L$ is the wavenumber corresponding to a single line defect and $\Lambda = c'(I)/(2c^2)$. The APD- and CV-restitution curves, $f(I)$ and $c(I)$, were calculated in a one-dimensional cable as in Ref. [17]. In addition, the intercellular coupling parameters ω and ξ were estimated as $\omega \sim 2\gamma/c$ and $\xi \sim (\gamma D)^{1/2}$ [17]. The comparison in Fig. 5 shows that the ring-based theory predicts reasonably well the frequency of line-defect rotation for anchored spiral waves of different period T , which was varied here by increasing the obstacle radius r_i in the simulations.

The opposite limit that can also be readily understood is the one where plane waves paced at the spiral rotation period exhibit line-defects that move towards the pacing site, which generally occurs for steeper CV-restitution. In this case, line-defect motion is expected to be dominated by the far-field spiral dynamics [17]. We have checked that, for the two-variable model of Ref. [17], spiral line-defects indeed rotate inward with a frequency equal to the product of the velocity of the planar line-defects and the inverse of their spacing. This property was purposely checked in a domain much larger than the spiral wavelength ($r_e = 18$ cm) and with an obstacle size ($r_i = 0.72$ cm) sufficient to prevent spiral wave breakup inherent in this model. However, we expect this behavior to be generic for systems with traveling planar line-defects and to also apply to freely rotating spirals with three line defects for parameters where breakup does not occur.

In summary, we have surveyed spiral line-defect patterns in simplified models of cardiac excitation with period-2 dynamics. Although far from exhaustive, this survey yields the striking finding that freely propagating and anchored spiral waves select different numbers of line-defects. This opens up the possibility to distinguish free and anchored spiral waves in cardiac tissue by monitoring the number of line-defects. We have shown that spiral wave unstable modes with different numbers of line-defects correspond to topologically quantized solutions of a Helmholtz equation. In this framework, the boundary condition on the period-2 oscillation amplitude in the spiral core, which is fundamentally different for free

and anchored spirals, is responsible for selecting the number of line defects. Furthermore, we have found that spiral line-defect inward rotation can be driven either by the core or far-field wavefront dynamics, with concomitantly different frequencies. Our results suggest that the observation of single-line-defect spirals in cardiac tissue culture [5, 6] may be a consequence of anchoring on small millimeter-size heterogeneities. However, the dynamics in real tissue is also influenced by the coupling of voltage and intracellular calcium dynamics [1, 4], which has been neglected here. The investigation of the effect of this coupling on line-defect dynamics and its relationship to wave breakup is an interesting future project. Finally, the previous finding of free spirals with one line-defect [21] in period-2 media with qualitatively different excitable dynamics than cardiac tissue suggests that other pattern selection mechanisms may be operative in different media. These differences also remain to be elucidated.

We thank Blas Echebarria for valuable discussions. This work was supported by NIH Grant No. P01 HL078931.

-
- [1] J. N. Weiss *et al.*, *Circulation* **112**, 1232 (2005).
 - [2] D. Barkley, *Phys. Rev. Lett.* **68**, 2090 (1992).
 - [3] V. Hakim and A. Karma, *Phys. Rev. Lett.* **79**, 665 (1997); *Phys. Rev. E* **60**, 5073-5105 (1999).
 - [4] A. Karma, and R. F. Gilmour, *Physics Today* **60**, 51 (2007); J. N. Weiss *et al.*, *Circ. Res.* **98**, 1244 (2006).
 - [5] S. M. Hwang, T. Y. Kim, and K. J. Lee, *Proc. Nat. Acad. of Sci. USA* **102**, 10363 (2005).
 - [6] T. Y. Kim *et al.*, *Proc. Natl. Acad. Sci. USA* **104**, 11639 (2007).
 - [7] J. S. Park, and K. J. Lee, *Phys. Rev. Lett.* **88**, 224501 (2002); J. S. Park, Sung-Jae Woo, and K. J. Lee, *Phys. Rev. Lett.* **93**, 098302 (2004); J. S. Park, and K. J. Lee, *Phys. Rev. E* **73**, 066219 (2006).
 - [8] J. S. Park, and K. J. Lee, *Phys. Rev. Lett.* **83**, 5393 (1999);
 - [9] B. Marts, D. J. W. Simpson, A. Hagberg, A. L. Lin, *Phys. Rev. E* **76**, 026213 (2007).
 - [10] A. Goryachev and R. Kapral, *Phys. Rev. E* **54**, 5469 (1996); A. Goryachev, H. Chaté, and R. Kapral, *Phys. Rev. Lett.* **80**, 873 (1998); A. Goryachev, R. Kapral, and H. Chaté, *Int. J. Bif. Chaos* **10**, 1537 (2000).
 - [11] S. Wu, *Fluc. and Noise Lett.* **6**, L379 (2006).
 - [12] J. S. Park, S.-J. Woo, O. Kwon, T. Y. Kim, and K. J. Lee, *Phys. Rev. Lett.* **100**, 068302 (2008).
 - [13] J. S. Park, and K. J. Lee, *Phys. Rev. Lett.* **83**, 5393 (1999);
 - [14] A. Karma, *Phys. Rev. Lett.* **71**, 1103 (1993).
 - [15] A. Karma, *Chaos* **4**, 461 (1994).
 - [16] F. H. Fenton *et al.*, *Chaos* **12**, 852 (2002).
 - [17] B. Echebarria and A. Karma, *Phys. Rev. Lett.* **88**, 208101 (2002); *Phys. Rev. E* **76**, 051911 (2007).
 - [18] M. A. Watanabe *et al.*, *J. Cardiovasc. Electrophysiol.* **12**, 196 (2001).
 - [19] B. Echebarria and A. Karma, *Eur. Phys. J. ST* **146**, 217 (2007).
 - [20] F. Fenton *et al.*, *Chaos* **15**, 013502 (2005).
 - [21] M. Zhan, and R. Kapral, *Phys. Rev. E* **72**, 046221 (2005).
 - [22] M. Courtemanche, L. Glass, and J. P. Keener, *Phys. Rev. Lett.* **70**, 2182 (1993).